

results further highlight the impact of catalyst on both reactivity and selectivity in the C–H borylation of light alkanes.

Overall, we have demonstrated that catalyst structure has a major impact on reaction rates and selectivities in the C–H borylation of methane. Over-functionalization of the initial product, CH<sub>3</sub>Bpin, can be limited through the appropriate selection of catalyst. These results open up exciting possibilities for catalyst design (to further modulate reactivity and selectivity in methane C–H borylation) as well as the application of the concepts delineated here for other light alkane C–H functionalization reactions.

## REFERENCES AND NOTES

- J. Choi, A. H. R. MacArthur, M. Brookhart, A. S. Goldman, *Chem. Rev.* **111**, 1761–1779 (2011).
- A. E. Shilov, G. B. Shul'pin, *Chem. Rev.* **97**, 2879–2932 (1997).
- T. Sakakura, T. Sodeyama, K. Sasaki, K. Wada, M. Tanaka, *J. Am. Chem. Soc.* **112**, 7221–7229 (1990).
- T. Ishiyama, N. Miyaura, *J. Organomet. Chem.* **680**, 3–11 (2003).
- I. A. I. Mkhaliid, J. H. Barnard, T. B. Marder, J. M. Murphy, J. F. Hartwig, *Chem. Rev.* **110**, 890–931 (2010).
- J. F. Hartwig, *Chem. Soc. Rev.* **40**, 1992–2002 (2011).
- J. F. Hartwig, *Acc. Chem. Res.* **45**, 864–873 (2012).
- H. M. L. Davies, J. R. Manning, *Nature* **451**, 417–424 (2008).
- D. Mansuy, *Coord. Chem. Rev.* **125**, 129–141 (1993).
- H. Schwarz, *Angew. Chem. Int. Ed.* **50**, 10096–10115 (2011).
- V. N. Cavalieri, B. F. Wicker, D. J. Mindiola, *Adv. Organomet. Chem.* **60**, 1–47 (2012).
- N. J. Gunsalus, M. M. Konnick, B. G. Hashiguchi, R. A. Periana, *Isr. J. Chem.* **54**, 1467–1480 (2014).
- P. Tang, Q. Zhu, Z. Wu, D. Ma, *Environ. Sci.* **7**, 2580–2591 (2014).
- A. Caballero, P. J. Pérez, *Chem. Soc. Rev.* **42**, 8809–8820 (2013).
- D. R. Lide, *CRC Handbook of Chemistry and Physics* (CRC Press, ed. 96, 2015).
- S. J. Blanksby, G. B. Ellison, *Acc. Chem. Res.* **36**, 255–263 (2003).
- A. Caballero *et al.*, *Science* **332**, 835–838 (2011).
- C. W. Liskay, J. F. Hartwig, *J. Am. Chem. Soc.* **134**, 12422–12425 (2012).
- C. W. Liskay, J. F. Hartwig, *J. Am. Chem. Soc.* **135**, 3375–3378 (2013).
- H. Chen, S. Schlecht, T. C. Semple, J. F. Hartwig, *Science* **287**, 1995–1997 (2000).
- C. S. Wei, C. A. Jiménez-Hoyos, M. F. Videá, J. F. Hartwig, M. B. Hall, *J. Am. Chem. Soc.* **132**, 3078–3091 (2010).
- J. F. Hartwig *et al.*, *J. Am. Chem. Soc.* **127**, 2538–2552 (2005).
- H. Chen, J. F. Hartwig, *Angew. Chem. Int. Ed.* **38**, 3391–3393 (1999).
- J. M. Murphy, J. D. Lawrence, K. Kawamura, C. Incarvito, J. F. Hartwig, *J. Am. Chem. Soc.* **128**, 13684–13685 (2006).
- Q. Li, C. W. Liskay, J. F. Hartwig, *J. Am. Chem. Soc.* **136**, 8755–8765 (2014).
- J. D. Lawrence, M. Takahashi, C. Bae, J. F. Hartwig, *J. Am. Chem. Soc.* **126**, 15334–15335 (2004).
- B. A. Vanchura II *et al.*, *Chem. Commun. (Camb.)* **46**, 7724–7726 (2010).
- H. Tajuddin *et al.*, *Chem. Sci.* **3**, 3505–3515 (2012).
- S. Shimada, A. S. Batsanov, J. A. K. Howard, T. B. Marder, *Angew. Chem. Int. Ed.* **40**, 2168–2171 (2001).
- M. A. Larsen, C. V. Wilson, J. F. Hartwig, *J. Am. Chem. Soc.* **137**, 8633–8643 (2015).
- These initial conditions were selected on the basis of (i) published conditions for alkane borylation reactions (20, 21, 24, 26) as well as (ii) the fixed volume of our Parr high-pressure reactor.
- The Ir-catalyzed background reaction of *c*-C<sub>5</sub>H<sub>10</sub> and *c*-C<sub>6</sub>H<sub>12</sub> with B<sub>2</sub>pin<sub>2</sub> in the absence of methane afforded 20.3 and 4.2% yield of the solvent C–H borylation products, respectively.
- G. A. Chotana *et al.*, *Chem. Commun. (Camb.)* **38**, 5731–5733 (2009).
- P. Nguyen, H. P. Blom, S. A. Westcott, N. J. Taylor, T. B. Marder, *J. Am. Chem. Soc.* **115**, 9329–9330 (1993).
- All three of these reactions passed the Hg drop test (supplementary materials), which is consistent with homogeneous catalysis.
- The concentrations of methane and ethane under the reaction conditions were determined by using Raman spectroscopic analysis of solutions of CH<sub>4</sub> or CH<sub>3</sub>CH<sub>3</sub> in C<sub>6</sub>D<sub>12</sub> (supplementary materials).
- M. Lin, T. E. Hogan, A. Sen, *J. Am. Chem. Soc.* **118**, 4574–4580 (1996).
- O. Demoulin, B. Le Clef, M. Navez, P. Ruiz, *Appl. Catal. A Gen.* **344**, 1–9 (2008).
- P. O. Graf, B. L. Mojet, L. Leferts, *Appl. Catal. A Gen.* **346**, 90–95 (2008).

## ACKNOWLEDGMENTS

The work conducted by A.K.C. (primarily involving evaluation of catalysts **1** and **2/3**) was supported by NSF under the Centers for Chemical Innovation (CCI) Center for Enabling New Technologies through Catalysis (CENTC) Phase II Renewal, CHE-1205189. The work conducted by S.D.S. (primarily involving evaluation of catalyst **4** and gas solubility measurements) was supported by the U.S. Department of Energy Office of Basic Energy Sciences (contract DE-FG02-08ER 15997). The Parr reactors used in this work were

purchased with funds from the NSF, under the CCI/CENTC Phase II Renewal, CHE-1205189. We gratefully acknowledge D. Samblanet for assistance with the gas solubility measurements. The University of Michigan has filed for a provisional patent on this work.

## SUPPLEMENTARY MATERIALS

www.sciencemag.org/content/351/6280/1421/suppl/DC1  
Materials and Methods  
Supplementary Text  
Figs. S1 to S19  
Tables S1 to S14  
References (40–57)

24 November 2015; accepted 18 February 2016  
10.1126/science.aad9289

## C–H BOND ACTIVATION

## Catalytic borylation of methane

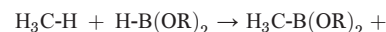
Kyle T. Smith,<sup>1</sup> Simon Berritt,<sup>1</sup> Mariano González-Moreiras,<sup>1</sup> Seihwan Ahn,<sup>2,3</sup> Milton R. Smith III,<sup>4\*</sup> Mu-Hyun Baik,<sup>2,3\*</sup> Daniel J. Mindiola<sup>1\*</sup>

Despite steady progress in catalytic methods for the borylation of hydrocarbons, methane has not yet been subject to this transformation. Here we report the iridium-catalyzed borylation of methane using bis(pinacolborane) in cyclohexane solvent. Initially, trace amounts of borylated products were detected with phenanthroline-coordinated Ir complexes. A combination of experimental high-pressure and high-throughput screening, and computational mechanism discovery techniques helped to rationalize the foundation of the catalysis and identify improved phosphine-coordinated catalytic complexes. Optimized conditions of 150°C and 3500-kilopascal pressure led to yields as high as ~52%, turnover numbers of 100, and improved chemoselectivity for monoborylated versus diborylated methane.

Activation of methane is challenging because it is nonpolar, has strong sp<sup>3</sup> C–H bonds, is sparingly soluble in both polar and nonpolar solvents, and has very high ionization energies and very low triple, boiling, and flashing points (*T*–*8*). Homogeneous catalysts that convert methane to products that could be used as liquid fuels are known, but these systems often require strong electrophiles and, in some cases, superacids and/or powerful oxidants (*1*, *2*, *9*–*17*). Chemoselectivity is another limitation in methane activation and functionalization. For instance, H<sub>3</sub>C–R (R = functional group) products resulting from methane activation and functionalization have more reactive C–H bonds than methane itself, hence often resulting in poor selectivity, overfunctionalization, and overoxidation.

The pioneering work by Hartwig, Marder, and Smith on C–H bond borylation inspired our investigation into the catalytic functionalization of methane using a similar approach (*18*). Whereas stoichiometric and catalytic borylations of alkanes show marked selectivity for monoborylation of terminal methyl groups (*18*), analogous reac-

tions with methane have not been thoroughly explored, despite this reaction being known for more than a decade. Fundamentally important is that the methyl-derived product is arguably a form of a mildly nucleophilic methyl transfer reagent, which complements the chemistry observed in electrophilic activation reactions in Shilov-type chemistry (*9*). Theory predicts that borylation of hydrocarbons with a borane (Eq. 1) is thermoneutral, whereas the weaker B–B bond in diboron reagents provides an enthalpic driving force of at least 12 kcal/mol, as shown in Eq. 2 (*18*). These considerations led us to pursue the catalytic borylation of methane using diboron reagents such as B<sub>2</sub>pin<sub>2</sub> (pin = pinacolate).



$$\text{H-H } \Delta H_o = -1 \text{ to } +1 \text{ kcal/mol} \quad (1)$$



$$\text{H-B(OR)}_2 \Delta H_o = -13 \text{ kcal/mol} \quad (2)$$

Iridium systems are particularly promising for C–H activation of methane (*1*, *2*), and some of the most active borylation catalysts use this transition metal (*18*). Therefore, we focused our attention on the commercially available iridium reagents [Ir(COD)(μ-Cl)]<sub>2</sub>, [Ir(COD)(μ-OMe)]<sub>2</sub> (COD = 1,5-cyclooctadiene), and (MesH)Ir(Bpin)<sub>3</sub> (MesH = mesitylene) (*19*), modifying them with a range of

<sup>1</sup>Department of Chemistry, University of Pennsylvania, 231 South 34th Street, Philadelphia, PA 19104, USA. <sup>2</sup>Institute for Basic Science—Center for Catalytic Hydrocarbon Functionalizations, Daejeon, Korea. <sup>3</sup>Department of Chemistry, Korea Advanced Institute of Science and Technology, Daejeon, Korea. <sup>4</sup>Department of Chemistry, Michigan State University, 578 South Shaw Lane, East Lansing, MI 48824, USA.  
\*Corresponding author. E-mail: smithm1@msu.edu (M.R.S.); mbaik2805@kaist.ac.kr (M.-H.B.); mindiola@sas.upenn.edu (D.J.M.)

nitrogen-based ligands, some of which are summarized in Table 1. Suitable catalyst and reaction conditions were identified systematically by means of a high-pressure, high-throughput reactor (see fig. S1 for details). Both  $[\text{Ir}(\text{COD})(\mu\text{-OMe})_2]$  and  $(\text{MesH})\text{Ir}(\text{Bpin})_3$  complexes gave some conversion to borylated methane products in cyclohexane (CyH) or tetrahydrofuran (THF) at pressures as low as 2068 kPa. Product yields were determined by gas chromatography–mass spectrometry (GC-MS) techniques with mesitylene as an internal standard.

$\text{Ir}(\text{I})$  precatalysts with supporting ligand combinations were exposed for 16 hours at 120°C to 2068 kPa of methane and  $\text{B}_2\text{pin}_2$ . Our results indicate that L3 (3,4,7,8-tetramethyl-1,10-phenanthroline) is the best nitrogen ligand. Among the products detected in the reaction mixture were  $\text{H}_3\text{CBpin}$  (**1**),  $\text{H}_2\text{C}[\text{Bpin}]_2$  (**2**),  $\text{HBpin}$  (**3**), and  $\text{H}_3\text{COBpin}$ . We also observed the production of  $\text{O}[\text{Bpin}]_2$ . Because hydrolysis of **1** and **2** is very slow on the basis of control experiments, we propose  $\text{O}[\text{Bpin}]_2$  to derive from a combination of hydrolysis of **3** during aerobic workup and analysis by GC-MS, as well as decomposition of  $\text{B}_2\text{pin}_2$  or **3**. The decomposition of  $\text{B}_2\text{pin}_2$  may be metal-catalyzed, as ring-opening of pinacolborane with Ir catalysts has been documented recently (20). We did not observe any tri- or tetraborylated methyl products,  $\text{H}_{4-x}\text{C}[\text{Bpin}]_x$  ( $x = 3$  or 4), whereas borylation of the solvent is barely detected under our conditions. Increasing  $\text{CH}_4$  pressures in small increments to 8274 kPa did not improve the mono- or diborylation reaction appreciably. Although gem-diborylation of alkanes is unknown, the gem-diborylation of benzylic groups has been documented (21, 22). Because three boryl moieties become incorporated into the active catalyst, as illustrated in Fig. 1, the diboron additive has an immediate impact on the reactivity. For instance, no reaction takes place when  $\text{B}_2\text{cat}_2$  (cat: catechol) is used instead of  $\text{B}_2\text{pin}_2$ , which is consistent with previous experimental and computational studies showing that borylation is favored for more electron-rich catalysts (23, 24).

The observed lower yield of **3** compared to **1** and **2** may be due to a second, slower borylation cycle that consumes **3** (Eq. 1). Consistent with our findings, we have observed that **3** can be used as a reactant replacing  $\text{B}_2(\text{pin})_2$ , but this reaction is much slower at 120°C (table S7). Other diboron reagents, such as  $\text{B}_2(\text{OH})_4$  or  $\text{B}_2(\text{NMe}_2)_4$ , produced complex mixtures of products with intractable precipitates.

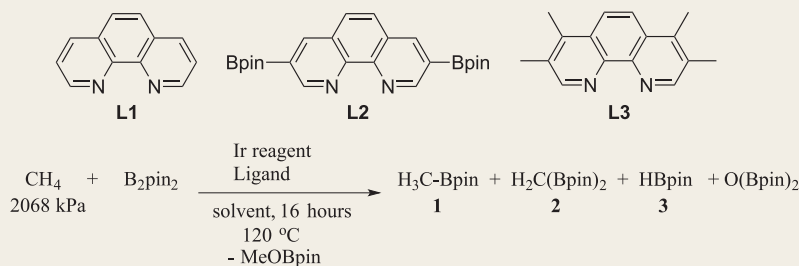
Table 1 summarizes some of our screening results with the most promising chelating polypyridyl ligands. The use of ligands L1 and L2 gave detectable amounts of  $\text{H}_3\text{CBpin}$ , whereas the best results were obtained with L3 (3,4,7,8-tetramethyl-1,10-phenanthroline), which showed yields as high as 4.1% and chemoselectivity ratios of mono- versus diborylated products **1**:**2** as high as 4:1. Surprisingly, even  $[\text{Ir}(\text{COD})(\mu\text{-OMe})_2]$  without exogenous ligand resulted in some borylation (<1%) but overall (25), the results listed in Table 1 suggest these systems to be stoichiometric with respect to methane borylation

(supplementary text). Likewise, increasing the temperature to 150°C did not improve the reaction (table S6).

The mechanism of methane borylation was modeled with density functional theory calculations

on the Ir-phenanthroline system, and the proposed catalytic cycle is summarized in Fig. 1. Before catalysis can take place, the  $[\text{Ir}(\text{COD})(\mu\text{-X})_2]$  ( $\text{X}^- = \text{OMe}$  or  $\text{Cl}$ ) undergoes a series of ligand substitutions to ultimately yield  $(\text{phen})\text{Ir}(\text{Bpin})_3$

**Table 1. 1,10-phenanthroline ligands used in the borylation of methane.** The ligands were added in a 2:1 ratio relative to dimeric Ir reagent and in a 1:1 ratio relative to independently prepared  $(\text{MesH})\text{Ir}(\text{Bpin})_3$ . Solvent was either tetrahydrofuran (THF) or cyclohexane (CyH). Results with other ligands are shown in table S4.



Entry	Ir reagent	Loading (mol %)	Ligand	Solvent	Percent yield 1	Ratio 1:2
1	$[\text{Ir}(\text{COD})(\mu\text{-OMe})_2]$	2.5	L3	THF	2.6	n/a
2	$[\text{Ir}(\text{COD})(\mu\text{-OMe})_2]$	5.0	L1	THF	1.5	n/a
3	$[\text{Ir}(\text{COD})(\mu\text{-OMe})_2]$	5.0	L2	THF	1.5	n/a
4	$[\text{Ir}(\text{COD})(\mu\text{-OMe})_2]$	5.0	L3	THF	2.7	n/a
5	$[\text{Ir}(\text{COD})(\mu\text{-OMe})_2]$	2.5	L3	CyH	2.0	3.9:1
6	$[\text{Ir}(\text{COD})(\mu\text{-OMe})_2]$	5.0	L3	CyH	2.3	2.5:1
7	$(\text{MesH})\text{Ir}(\text{Bpin})_3$	2.5	L3	THF	4.1	n/a
8	$(\text{MesH})\text{Ir}(\text{Bpin})_3$	5.0	L5	THF	2.4	n/a
9	$(\text{MesH})\text{Ir}(\text{Bpin})_3$	2.5	L5	CyH	1.7	2.9:1

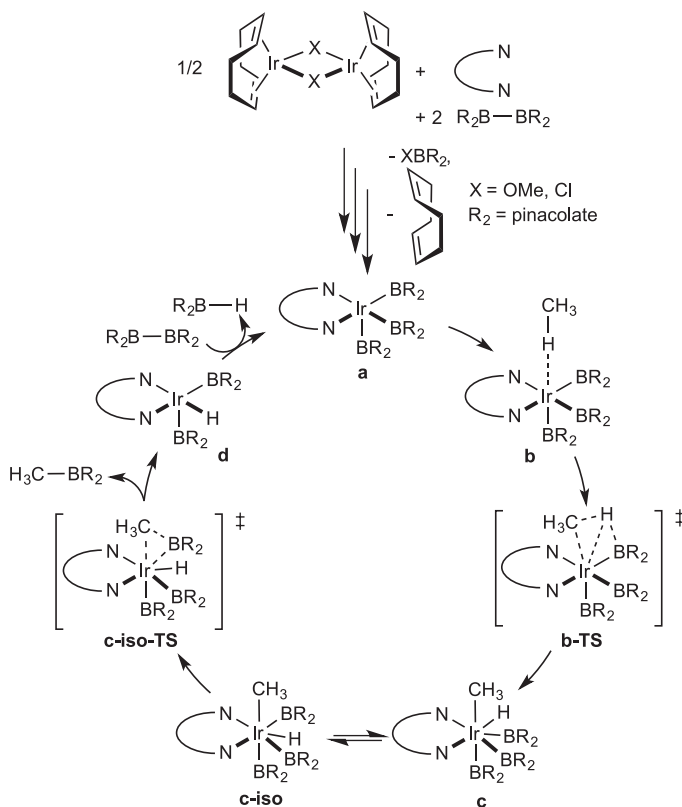


**Fig. 1. Proposed cycle for the monoborylation of methane with 1,10-phenanthroline as a supporting ligand.**

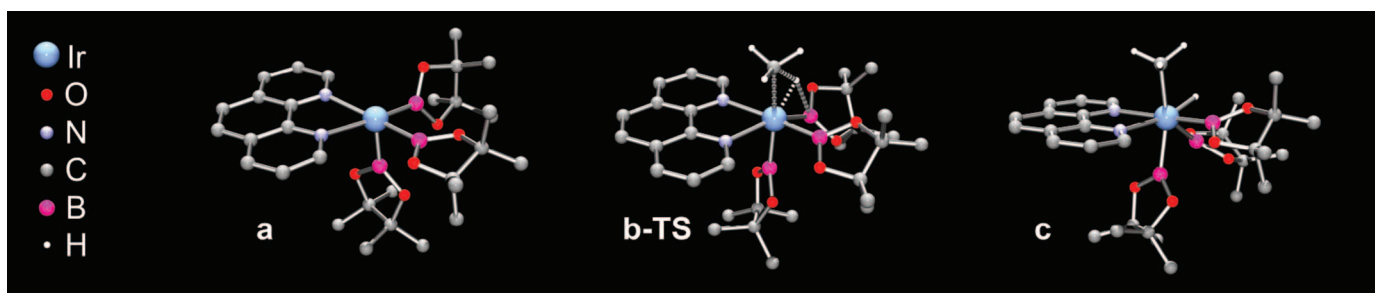
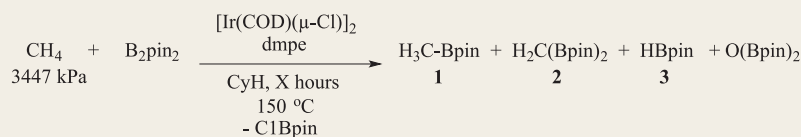


Fig. 2. Computed structures of catalytic cycle states in Fig. 1. Nonessential hydrogens are omitted for clarity.

**Table 2. Variations of catalyst loading and time with the ligand dmpe for the borylation of methane.** The ligand dmpe ( $\text{Me}_2\text{PCH}_2\text{CH}_2\text{PMe}_2$ ) was used in a 2:1 ratio relative to the Ir precatalyst  $[\text{Ir}(\text{COD})(\mu\text{-Cl})_2]$  in cyclohexane (CyH) under 3447 kPa of  $\text{CH}_4$ .



Entry	Loading (mol %)	Time (hours)	Percent yield 1	1:2	TON
1	25	16	9.4	9:1	<1
2	10	16	16	5:1	~1
3	5.0	16	23	5:1	4
4	1.0	16	25	5:1	25
5	0.5	16	52	3:1	104
6	25	6	17	7:1	<1
7	10	6	25	7:1	~2
8	5.0	6	27	6:1	5
9	1.0	6	21	8:1	21
10	0.5	6	28	6:1	56
11	10	2	22	3:1	22
12	5.0	2	27	4:1	5
13	1.0	2	24	4:1	24
14	0.5	2	16	2:1	32

(phen = 1,10-phenanthroline). This complex is the most plausible resting state of the catalyst and consists of an Ir(III)- $d^6$  center in a pseudo-square-pyramidal coordination geometry labeled as **a** (see Fig. 2). The catalytic cycle commences with weak binding of methane at the empty coordination site to give the intermediate complex **b**, followed by oxidative addition traversing the likely rate-determining transition state **b-TS** at 25.9 kcal/mol (26). The iridium center in this intermediate **c** adopts a rare, but not unprecedented, seven-coordinate geometry (27). Next, the hydride and borane ligands swap position to give access to **c-iso** that can undergo reductive elimination of the boryl-methane product **1** to afford the Ir(III)-complex **d**, which reacts with another equivalent of the diboron source to regenerate the catalyst resting state **a**. We considered several alternative mechanisms, most notably a  $\sigma$ -bond metathesis pathway (28), but found that the mechanism shown

in Fig. 1 is energetically most favorable. A detailed analysis of the computational results suggested a potential optimization strategy: As the H- $\text{CH}_3$  bond is cleaved at the transition state **b-TS**, the Ir-center must undergo formally an oxidation from Ir(III) to Ir(V). Therefore, the hard N-based Lewis base ligands may not provide the ideal supporting ligand framework, as these ligands tend to decrease the polarizability of the valence electrons of the metal. Softer Lewis bases, such as the phosphine analogs of the N ligands, seemed likely to prove beneficial by increasing the polarizability of the metal.

We tested the simple qualitative rationale from our computer model by exploring whether phosphine ligands offered improved reactivity toward C-B bond formation. Initial screens showed that phosphine ligands do not result in any notable borylation at 120°C with 2068 to 3447 kPa of methane, but at 150°C the dmpe

ligand ( $\text{Me}_2\text{PCH}_2\text{CH}_2\text{PMe}_2$ ) improved the reaction substantially. Table 2 summarizes the best results from our screening. Varying catalyst loadings from 0.5 to 25 mole percent (mol %) led to conversion yields as high as 52% and catalytic turnover numbers (TONs) up to 104 with selectivity of 3:1 for monoborylated product **1** versus **2**. Increasing the mol % of catalyst resulted in lower conversion, though the selectivity for mono- versus diborylation (**1:2** ratio) of methane increased to as high as 9:1 (entry 1). Pressures below 1379 kPa afforded lower conversions, whereas pressures above 3447 kPa did not greatly improve the overall yield of products. Reactions required 16 hours for completion, and control experiments using similar amounts of dmpe/ $[\text{Ir}(\text{COD})(\mu\text{-Cl})_2]$  and **1** as a reagent with 40 equivalents of  $\text{B}_2(\text{pin})_2$  (with or without methane) did yield the diborylated product **2**. This result implies that the yield of monoborylation product is always greater than for diborylation with the dmpe scaffold.

An inverse relationship between precatalyst concentration and borylation conversion has previously been observed in borylations with  $[\text{Ir}(\text{COD})(\mu\text{-Cl})_2]$  precatalysts and N-chelating ligands, but no explanation was provided for this behavior (29). Recently, Finke and co-workers have analyzed similar counterintuitive behavior in hydrogenations with Ziegler-type nanoparticle catalysts prepared from Ir precatalysts (30). Likewise, benzene borylation has been described with Ir nanoparticles at 80°C with activities that are considerably lower than those for homogeneous catalysts (31). Both of these Ir nanoparticle-catalyzed reactions are poisoned by Hg. In our case, Hg addition to the reactions listed in Table 2 did not suppress catalysis. In addition, borylations with dmpe and phenanthroline-based ligands at 150°C with identical precatalyst loadings and concentrations give very different conversions (table S6). These observations are consistent with a homogeneous process in which the nature of the ligand affects catalysis. Lastly, methane activation over Ir/ZrO<sub>2</sub> has been described, but high temperatures (~600°C) are typically required for these processes (32).

Because dmpe/ $[\text{Ir}(\text{COD})(\mu\text{-Cl})_2]$  afforded the cleanest yield of monoborylated product **1**, we conducted isotopic labeling studies using <sup>13</sup>CH<sub>4</sub>-enriched methane (99% atom enriched, 1379 kPa) to unambiguously establish that methane gas is the source of methyl in **1**. As anticipated, GC-MS results conclusively established the formation of

$I$ - $^{13}\text{C}$  as the only product derived from  $^{13}\text{CH}_4$  borylation (fig. S7), excluding the possibility of pinacol or solvent degradation as possible sources of  $\text{CH}_3$ . Mechanistically, we expect the phosphine system to follow the same route outlined above for the polypyridyl systems.

## REFERENCES AND NOTES

- V. N. Cavaliere, B. F. Wicker, D. J. Minciola, *Adv. Organomet. Chem.* **60**, 1–47 (2012).
- V. N. Cavaliere, D. J. Minciola, *Chem. Sci.* **3**, 3356–3365 (2012).
- R. H. Crabtree, *Chem. Rev.* **85**, 245–269 (1985).
- G. Parshall, *Homogeneous Catalysis* (Wiley, New York, 1982).
- H. Arakawa et al., *Chem. Rev.* **101**, 953–996 (2001).
- W. A. Chupka, J. Berkowitz, *J. Chem. Phys.* **54**, 4256–4266 (1971).
- J. Berkowitz, J. P. Greene, H. Cho, B. Ruscic, *J. Chem. Phys.* **86**, 674–676 (1987).
- S. J. Blanksby, G. B. Ellison, *Acc. Chem. Res.* **36**, 255–263 (2003).
- A. E. Shilov, G. B. Shul'pin, *Chem. Rev.* **97**, 2879–2932 (1997).
- A. Caballero, P. J. Pérez, *Chem. Soc. Rev.* **42**, 8809–8820 (2013).
- R. A. Periana et al., *Science* **280**, 560–564 (1998).
- R. A. Periana, O. Mironov, D. Taube, G. Bhalla, C. J. Jones, *Science* **301**, 814–818 (2003).
- A. D. Sadow, T. D. Tilley, *Angew. Chem. Int. Ed.* **42**, 803–805 (2003).
- A. D. Sadow, T. D. Tilley, *J. Am. Chem. Soc.* **127**, 643–656 (2005).
- M. V. Kirilova et al., *J. Am. Chem. Soc.* **129**, 10531–10545 (2007).
- A. Caballero et al., *Science* **332**, 835–838 (2011).
- M. Lin, A. Sen, *Nature* **368**, 613–615 (1994).
- I. A. I. Mkhaliid, J. H. Barnard, T. B. Marder, J. M. Murphy, J. F. Hartwig, *Chem. Rev.* **110**, 890–931 (2010).
- G. A. Chotana et al., *Chem. Commun. (Camb.)* **45**, 5731–5733 (2009).
- B. Ghaffari et al., *Organometallics* **34**, 4732–4740 (2015).
- S. Shimada, A. S. Batsanov, J. A. K. Howard, T. B. Marder, *Angew. Chem. Int. Ed.* **40**, 2168–2171 (2001).
- W. N. Palmer, J. V. Obligation, I. Pappas, P. J. Chirik, *J. Am. Chem. Soc.* **138**, 766–769 (2016).
- C. W. Liskey, C. S. Wei, D. R. Pahls, J. F. Hartwig, *Chem. Commun. (Camb.)* **45**, 5603–5605 (2009).
- B. A. Vanchura II et al., *Chem. Commun. (Camb.)* **46**, 7724–7726 (2010).
- P. Nguyen, H. P. Blom, S. A. Westcott, N. J. Taylor, T. B. Marder, *J. Am. Chem. Soc.* **115**, 9329–9330 (1993).
- All energies discussed are obtained from calculations without any corrections for concentration differences. That is, all calculations assume standard conditions. In reality, the substrate concentrations are a few orders of magnitude higher than the concentration of the catalyst. Thus, Le Chatelier's principle will give rise to a lowering of all free energies by a few kcal/mol. As a result, our computed barrier of 25.9 kcal/mol must be considered an upper bound estimate. The real barrier will be a few kcal/mol lower because of the concentration differential.
- H. Tamura, H. Yamazaki, H. Sato, S. Sakaki, *J. Am. Chem. Soc.* **125**, 16114–16126 (2003).
- Q. Li, C. W. Liskey, J. F. Hartwig, *J. Am. Chem. Soc.* **136**, 8755–8765 (2014).
- T. Tagata, M. Nishida, *Adv. Synth. Catal.* **346**, 1655–1660 (2004).
- A. B. Crooks et al., *ACS Catalysis* **5**, 3342–3353 (2015).
- Z. Yinghuai et al., *Inorg. Chem.* **47**, 5756–5761 (2008).
- J. Wei, E. Iglesia, *Angew. Chem. Int. Ed.* **43**, 3685–3688 (2004).

## ACKNOWLEDGMENTS

A U.S. provisional patent has been filed for this work. Financial support of this research was provided to D.J.M. by the University of Pennsylvania. M.G.-M. thanks the Ministry of Education of Spain for sponsoring his work in the United States. M.-H.B. thanks the Institute for Basic Science (IBS-R10-D1) in Korea for support. M.R.S. thanks the NIH (GM63188) for support. We thank B. Ghaffari and K. Gore for providing some catalysts and ligands and B.-C. Lee for help in some catalytic reactions. Experimental procedures, spectroscopic measurements, and theoretical calculations are provided in the supplementary materials.

## SUPPLEMENTARY MATERIALS

www.sciencemag.org/content/351/6280/1424/suppl/DC1  
Materials and Methods  
Supplementary Text  
Figs. S1 to S15  
Tables S1 to S8  
References (33–43)

30 November 2015; accepted 18 February 2016  
10.1126/science.aad9730

## MAGNETOHYDRODYNAMICS

# Large-scale magnetic fields at high Reynolds numbers in magnetohydrodynamic simulations

H. Hotta,<sup>1,2\*</sup> M. Rempel,<sup>2</sup> T. Yokoyama<sup>3</sup>

The 11-year solar magnetic cycle shows a high degree of coherence in spite of the turbulent nature of the solar convection zone. It has been found in recent high-resolution magnetohydrodynamics simulations that the maintenance of a large-scale coherent magnetic field is difficult with small viscosity and magnetic diffusivity ( $\lesssim 10^{12}$  square centimeters per second). We reproduced previous findings that indicate a reduction of the energy in the large-scale magnetic field for lower diffusivities and demonstrate the recovery of the global-scale magnetic field using unprecedentedly high resolution. We found an efficient small-scale dynamo that suppresses small-scale flows, which mimics the properties of large diffusivity. As a result, the global-scale magnetic field is maintained even in the regime of small diffusivities—that is, large Reynolds numbers.

The Sun shows an 11-year magnetic activity cycle that exhibits a large degree of coherence. The Sun's activity has been recorded in terms of number of sunspots, whose record has a long observation history dating from 1610 (1). The coherence of the large-scale field is evident from the 11-year polar field reversals and parity rules of sunspot pairs (2) that show only very few violations. The solar magnetic field and its cyclic activity is thought to be maintained by dynamo action: the transformation of kinetic energy to magnetic energy by the turbulent motion of the ionized plasma in the solar convection zone (3). A remaining mystery is the generation process of the coherent large-scale magnetic field in the presence of chaotic small-scale fields, which are expected because of the large magnetic and fluid Reynolds numbers of the solar convection zone. Some studies have already succeeded in reproducing a magnetic cycle in three-dimensional (3D) convection calculations (4–6). Recent calculations, however, suggest that large fluid and magnetic Reynolds numbers—small viscosity and magnetic diffusivity—lead to a reduction of the energy and coherence of the global-scale magnetic field (7). 2.5D kinematic dynamo calculations with high magnetic Reynolds numbers suggest that the construction of the global-scale magnetic field requires the suppression of the small-scale dynamo (8, 9). Although the suppression of the small-scale dynamo is caused by the strong shear in these investigations, they suggested a possibility of the nonlinear Lorentz feedback that can suppress the small-scale phenomena and cannot be included in these investigations because of kinematic assumption—that is, ignoring the Lorentz force. The global dynamo cal-

culations that show the coherent global-scale magnetic field (4–6) use relatively large viscosity and magnetic diffusivity ( $\geq 10^{12}$  cm<sup>2</sup> s<sup>-1</sup> in solar cases) or small number of grid points in ILES (implicit large-eddy simulation) approaches in order to suppress the small-scale chaotic magnetic field. However, the sun has very small viscosity and magnetic diffusivity (1 and 10<sup>4</sup> cm<sup>2</sup> s<sup>-1</sup> at the base of the convection zone, respectively) (10, 11). Thus, we need to understand the construction mechanism of the global-scale magnetic field in the presence of small viscosity and diffusivity.

A hint is seen in recent high-resolution calculations for the small-scale dynamo in the solar convection zone (12). For sufficiently high resolution, the small-scale dynamo becomes efficient, and the magnetic energy exceeds the kinetic energy on small scales. Then, the Lorentz force feedback becomes significant—the kinematic assumption is no longer valid, and the small-scale flow is suppressed. This process requires a high resolution to resolve the inertial scale of the turbulence well. Because of the substantial scale separation between the global scale of the sun (circumference is  $4.4 \times 10^9$  m) and the energy injection scale of the turbulence (density scale height is  $6 \times 10^7$  m at the base of the convection zone), resolving an efficient small-scale dynamo in global simulations requires a large number of grid points and/or efficient numerical schemes that resolve small-scale turbulence.

Here, we present high-resolution calculations that resolve the turbulence inertial scale well and maintain an efficient small-scale dynamo even in the global domain. We adopt the reduced speed of sound technique (13) and solve the 3D magnetohydrodynamics equations in spherical geometry ( $r, \theta, \phi$ ) with gravity and rotation. The solar standard model (Model S) is used for the background stratification (14). We have previously performed similar calculations, but without rotation (15) or magnetic field (16). In addition, the calculation time is much longer in this study. In

<sup>1</sup>Department of Physics, Graduate School of Science, Chiba University, 1-33 Yayoi-cho, Inage-ku, Chiba 263-8522, Japan.

<sup>2</sup>High Altitude Observatory, National Center for Atmospheric Research (NCAR), Post Office Box 3000, Boulder, CO 80307, USA.

<sup>3</sup>Department of Earth and Planetary Science, University of Tokyo, 7-3-1, Hongo, Bunkyo-ku, Tokyo, 113-0033, Japan.

\*Corresponding author. E-mail: hotta@chiba-u.jp



## Catalytic borylation of methane

Kyle T. Smith *et al.*

*Science* **351**, 1424 (2016);

DOI: 10.1126/science.aad9730

---

*This copy is for your personal, non-commercial use only.*

---

**If you wish to distribute this article to others**, you can order high-quality copies for your colleagues, clients, or customers by [clicking here](#).

**Permission to republish or repurpose articles or portions of articles** can be obtained by following the guidelines [here](#).

**The following resources related to this article are available online at [www.sciencemag.org](http://www.sciencemag.org) (this information is current as of March 25, 2016 ):**

**Updated information and services**, including high-resolution figures, can be found in the online version of this article at:

</content/351/6280/1424.full.html>

**Supporting Online Material** can be found at:

</content/suppl/2016/03/23/351.6280.1424.DC1.html>

This article **cites 40 articles**, 3 of which can be accessed free:

</content/351/6280/1424.full.html#ref-list-1>

This article appears in the following **subject collections**:

Chemistry

</cgi/collection/chemistry>